

# TOWARDS NEURAL SCALING LAWS FOR TIME SERIES FOUNDATION MODELS

Qingren Yao<sup>1,2</sup>, Chao-Han Huck Yang<sup>3</sup>, Renhe Jiang<sup>4</sup>, Yuxuan Liang<sup>2\*</sup>, Ming Jin<sup>1\*</sup>, Shirui Pan<sup>1</sup>

<sup>1</sup>Griffith University <sup>2</sup>The Hong Kong University of Science and Technology (Guangzhou)

<sup>3</sup>NVIDIA Research <sup>4</sup>The University of Tokyo

## ABSTRACT

Scaling laws offer valuable insights into the design of time series foundation models (TSFMs). However, previous research has largely focused on the scaling laws of TSFMs for in-distribution (ID) data, leaving their out-of-distribution (OOD) scaling behavior and the influence of model architectures less explored. In this work, we examine two common TSFM architectures—encoder-only and decoder-only Transformers—and investigate their scaling behavior on both ID and OOD data. These models are trained and evaluated across varying parameter counts, compute budgets, and dataset sizes. Our experiments reveal that the log-likelihood loss of TSFMs exhibits similar scaling behavior in both OOD and ID settings. We further compare the scaling properties across different architectures, incorporating two state-of-the-art TSFMs as case studies, showing that model architecture plays a significant role in scaling. The encoder-only Transformers demonstrate better scalability than the decoder-only Transformers, while the architectural enhancements in the two advanced TSFMs primarily improve ID performance but reduce OOD scalability. While scaling up TSFMs is expected to drive performance breakthroughs, the lack of a comprehensive understanding of TSFM scaling laws has hindered the development of a robust framework to guide model scaling. We fill this gap in this work by synthesizing our findings and providing practical guidelines for designing and scaling larger TSFMs with enhanced model capabilities.

## 1 INTRODUCTION

Time series analysis is an important piece of data mining, facilitating decision-making and scientific inference across various domains (Zhang et al., 2023). As an important analysis task, time series forecasting has long been studied and drives a wide range of practical applications, from energy, climate and quantitative finance to urban computing and system management (Jin et al., 2023; Nie et al., 2024; Wen et al., 2024). Various methods have been proposed for this task, ranging from classical statistic models (Hyndman & Athanasopoulos, 2013), bespoke dynamical models (Prado, 2020), to the more recent deep-learning based approaches (Wen et al., 2022). Despite their competitive performance, the methods are typically designed for specific tasks, poor to generalize to other domains (Fan et al., 2023; Rasul et al., 2023). Concurrently, we are witnessing a paradigm shift in time series forecasting from task-specific models to universal models, with the emergence of time series foundation models (TSFMs). Timer (Liu et al., 2024), Moirai (Woo et al., 2024), and more recently proposed Time-MoE (Shi et al., 2024b) show trends of scaling in both data volume and model size, aiming to achieve performance breakthroughs through more resource investment.

The neural scaling law quantitatively describes how model performance grows with the scaling of three basic training factors: model parameters, computational resources and training dataset size. Establishing such scaling laws is crucial for developing TSFMs, as it provides a framework for predicting expected performance gains, enabling the community to rationally allocate efforts toward key designs. The exploration on scaling laws for TSFMs is still in an initial stage; recent research has primarily focused on studying ID scaling behavior (Edwards et al., 2024; Shi et al., 2024a). In practical applications, TSFMs primarily face challenges from unseen scenarios (Wang et al., 2024),

\*Correspondence to: Y. Liang <yuxliang@outlook.com> and M. Jin <mingjinedu@gmail.com>

where OOD forecasting capability is most critical. This raises an unresolved question: *do neural scaling laws also apply to predict out-of-distribution forecasting performance?* Moreover, various architectures of TSFMs have been arising, but they typically focus on performance improvement at specific scales. No studies have investigated the scaling behaviors across different architectures, leaving a key question unanswered: *how do model architectures affect scalability?* Although we are seeing an increasing investment in training resources for TSFMs, the bottlenecks and potential driving factors for developing larger TSFMs remain unclear. This raises another practical question: *how to design TSFMs from the perspective of scalability?*

In this paper, we aim to provide empirical answers to the above research questions. To investigate the scaling laws in OOD scenarios, we trained a family of encoder-only Transformer-based TSFMs, varying three basic training factors: model sizes, compute budgets, and training set sizes. We evaluated their performance on both ID and OOD test sets and established scaling laws for three training factors in each scenario. To examine the impact of model architecture on scaling behavior, we trained decoder-only Transformer based TSFMs and compared them with the encoder-only versions. Additionally, we included two state-of-the-art TSFMs, Moirai (Woo et al., 2024) and Chronos (Ansari et al., 2024), as case studies for detailed analysis. Our experiment results suggest that the log-likelihood loss of TSFMs exhibits similar scaling behavior in both OOD and ID scenarios; encoder-only Transformer has better scalability than decoder-only Transformer; the architectural modifications introduced by two advanced TSFMs mainly improve ID performance but compromise OOD scalability. Based on the findings and comparative analysis, we finally provided design principles for TSFMs from a scaling perspective.

Our contributions are summarized as follows:

- **Scaling laws across data distributions.** We extend the scaling laws for TSFMs from ID scenarios to OOD scenarios across three core training factors: model size, computational resources, and dataset size, establishing a foundation for predicting expected OOD performance gains of TSFMs.
- **Scaling laws across model architectures.** We investigate the scaling patterns of different architectures of TSFMs, offering some insights for scalable TSFM design.
- **Scaling laws-guided design principles.** We provide practical design principles for TSFMs from the perspective of data, model and compute scaling, via analyzing the commonalities and differences in scaling behaviors across data distributions and model architectures

## 2 PRELIMINARY

To investigate the scaling laws of TSFMs, we curated a large, diverse, and balanced dataset for pre-training. Leveraging this dataset, we trained both *encoder-only* and *decoder-only* transformers and two state-of-the-art TSFMs: Chronos and Moirai. For comparative analysis, we evaluated these models on (i) *in-distribution* and (ii) *out-of-distribution* test sets, focusing on key performance metrics to examine the scaling behavior across architectures.

### 2.1 DATASETS

A large scale, diverse, balanced and high quality pre-training dataset is the foundation to build FMs. To this end, we constructed our time series corpus for TSFM pre-training from the large-scale open time series archive, Lotsa (Woo et al., 2024). The corpus comprises approximately 15B time points from 39 datasets spanning seven distinct domains. To ensure that the model performs fairly across all domains, we maintained a balanced ratio of data from different domains. Furthermore, we performed quality filtering on the corpus by constraining the signal-to-noise ratio of a time series to be greater than 20 dB, ensuring that the pre-training corpus exhibits strong predictability. A detailed breakdown of the data sources is provided in Appendix A, with a summary in Table 1.

Table 1: **Dataset summary.** M indicates million and B indicates billion.

Domain	Transport	Climate	Energy	CloudOps	Health	Sales	Web	Sum
Datasets	8	2	14	3	9	1	2	39
Time points	4.82B	4.73B	2.34B	2.15B	240M	140M	600M	14.46B
Proportion	33.31%	32.71%	16.15%	14.86%	1.61%	0.96%	0.40%	100%

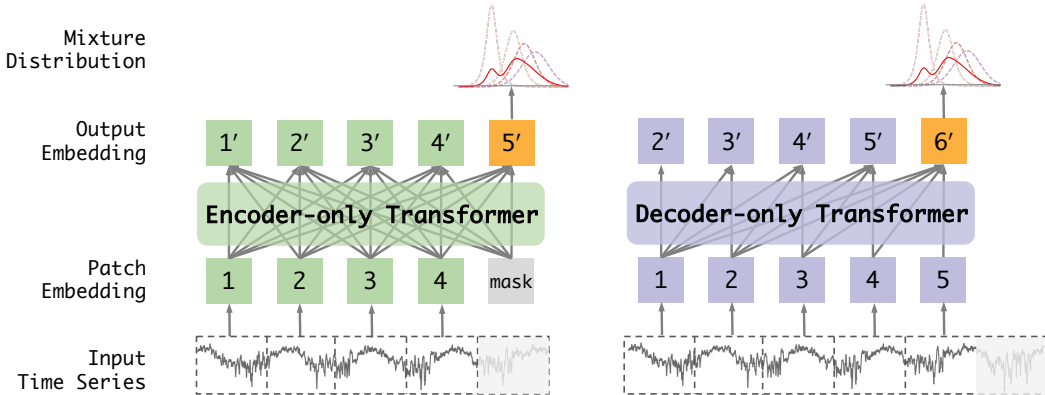


Figure 1: **Architectures of Baseline Time Series Foundation Models.** The the most widely used two Transformer architectures, encoder-only Transformer and decoder-only Transformer, are selected to be our baselines. The time series is divided into patches, each treated as a token input to the Transformer model. Shaded patches represent the future horizon to be predicted.

To assess the impact of pre-training data scale on model performance, we partitioned the corpus into subsets containing 10M, 100M, and 1B time points, ensuring that each subset maintained similar diversity. For each subset, 95% of the data was allocated for model training, with the remaining 5% reserved as a validation set to evaluate *in-distribution* forecasting performance. Additionally, we used a subset from a widely recognized long-sequence prediction benchmark (Wu et al., 2023) to test the model’s *out-of-distribution* forecasting capabilities. This subset includes test data from the ETTh1-2, ETTm1-2, electricity, and weather datasets.

## 2.2 MODELS

TSFMs are predominantly built upon the Transformer architecture (Wen et al., 2022). For our baseline models, we selected two widely adopted architectures: the encoder-only Transformers and the decoder-only Transformers. We also include the state-of-the-art models from both architectures, Moirai (Woo et al., 2024) (encoder-only) and Chronos (Ansari et al., 2024) (decoder-only), in our study for comparison. Although Chronos-T5 is technically an encoder-decoder Transformer, we categorize it as analogous to decoder-only Transformers because it primarily relies on the decoder’s auto-regressive method for prediction. The primary distinction between encoder-only and decoder-only architectures lies in the attention mechanisms applied to the inputs, as illustrated in Figure 1. To better adapt them for time series forecasting, we introduce three key modifications in input layer, positional encoding and prediction head. More details are given in appendix B.

**Patch Embedding.** There are several approaches for generating inputs for transformer-based TSFMs, including point embedding, patch embedding, and lagged feature embedding. Due to the high computational cost of point embedding for long sequences and the limited robustness of lagged feature embedding, we adopt patch embedding in our models. This method, initially introduced by Vision Transformers (Dosovitskiy et al., 2020) and later adapted by PatchTST (Nie et al., 2023) for time series forecasting, divides the time series into non-overlapping segments, which are then projected into a feature space.

**Rotary Position Embedding.** This technique (RoPE) has rapidly gained popularity as a positional encoding method in recent large language models (Su et al., 2024). Given its proven effectiveness in improving time series forecasting performance (Woo et al., 2023), we adopt RoPE as a replacement for the original Transformer’s positional encoding. RoPE encodes absolute positions using a rotation matrix while embedding relative position dependencies directly into the self-attention mechanism.

**Mixture of Distributions.** Our models are designed to predict the probability distribution of future time series. However, real-world time series often exhibit complex distributions, including outliers, heavy tails, and extreme skew, which pose significant challenges for accurate modeling. To address

these complexities, we incorporate a more flexible output likelihood by utilizing Student-t mixture models (Flunkert et al., 2017). Compared to the commonly used Gaussian mixture models, Student-t mixture models offer greater robustness in handling outliers and heavy-tailed distributions.

Our models are characterized by several key hyperparameters: the number of layers ( $n_{\text{layer}}$ ), the input/output dimensions of the residual stream ( $d_m$ ), the dimensions of the intermediate feed-forward layers ( $d_{\text{ff}}$ ), the number of attention heads per layer ( $n_{\text{heads}}$ ), and the dimension of the attention output ( $d_{\text{head}}$ ). The overall model size can be expressed as:

$$\begin{aligned} N &\approx n_{\text{layer}} (4d_m n_{\text{heads}} d_{\text{head}} + 2d_m * d_{\text{ff}}) \\ &= 2d_m n_{\text{layer}} (2n_{\text{heads}} d_{\text{head}} + d_{\text{ff}}) \\ &= 12n_{\text{layer}} d_m^2 \quad \text{with the standard} \quad n_{\text{head}} \cdot d_{\text{head}} = d_m = d_{\text{ff}}/4, \end{aligned} \tag{1}$$

where the embedding layer, prediction head, biases and other sub-leading terms are excluded for a cleaner scaling laws. The embedding layer uses a patch size of 32 with  $32d_m$  parameters. The mixture distribution prediction head comprises multiple independent linear layers that predict the Student-t mixture distribution parameters for each patch, with  $512d_m$  parameters in total. In the study, we explore models with  $\sim 10^3$  to  $\sim 10^8$  trainable parameters.

### 2.3 TRAINING AND EVALUATION DETAILS

In this study, we focus exclusively on univariate time series forecasting to avoid the confounding effects introduced by multivariate time series, such as variable interactions, correlations, and the complexities of modeling multivariate relationships. Future research will address these factors, aiming to establish more comprehensive scaling laws for multivariate time series models.

**Training Details.** Our training objective is to optimize the mixture distribution log-likelihood. We utilize the AdamW optimizer with a batch size of 128 and a cosine learning rate scheduler with a linear warm-up of  $10^4$  training steps, training for a total of  $10^5$  steps. To facilitate learning data representations across diverse domains with varying series lengths and sample sizes, we visited each sample with probability  $p_i = t_i/T$ , where  $t_i$  is the series’ time points and  $T$  is the corpus’ total time points. We then randomly selected a segment from each chosen sample.

**Evaluation Details.** We evaluate the model on a randomly selected 10% subset of the test data every  $10^3$  steps to reduce computational costs. For performance measurement, we observed that non-normalized metrics like MAE and MSE are highly sensitive to the amplitude of time series data, often causing the overall average to be disproportionately influenced by high-amplitude datasets. To mitigate this issue, we utilize the normalized metric, mean absolute percentage error (MAPE), along with the log-likelihood loss, to assess forecasting performance. Detailed descriptions of these metrics are provided in the Appendix C.3.

## 3 SCALING LAWS FOR TIME SERIES FOUNDATION MODELS

In this section, we first present experimental results using the encoder-only Transformer to explore scaling laws across different data distributions. Following this, we conduct a comparative study on the scaling behavior of encoder-only and decoder-only TSFMs, Moirai and Chronos, to investigate how model architectures influence the scalability of time series models.

### 3.1 SCALING LAWS ACROSS DATA DISTRIBUTIONS

**Parameter Scaling.** In Figure 2, we display the ID and OOD performance of a wide variety of encoder-only Transformers, ranging from small models with 3K parameters to large models with 300M parameters. We trained models on the full 15B pre-training corpus to convergence and report the minimum log-likelihood loss and MAPE. We can see that both ID and OOD performance roughly follow power-law behavior over five orders of magnitude in model sizes. Formally, the power law can be expressed as:

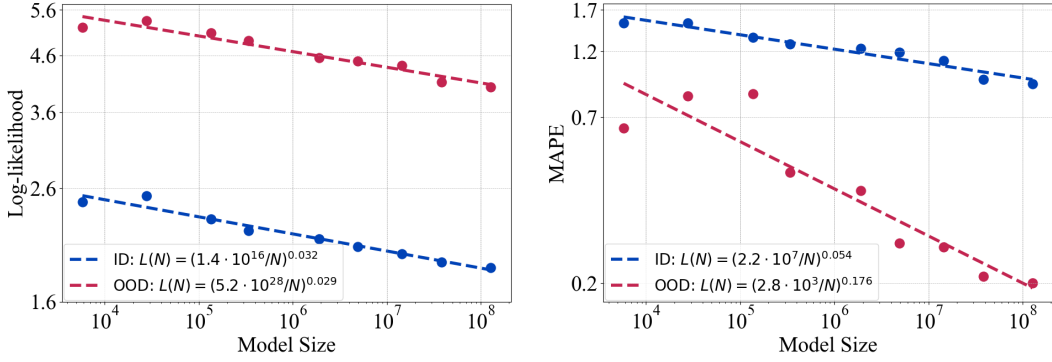


Figure 2: **Parameter Scaling.** The scaling effect of trainable model parameters on the in-distribution (ID) and out-of-distribution (OOD) forecasting performance, which is evaluated using log-likelihood and MAPE metrics. When evaluated with log-likelihood, both ID and OOD results follow an approximate power law scaling with parameter count, exhibiting consistent trends across different data distributions.

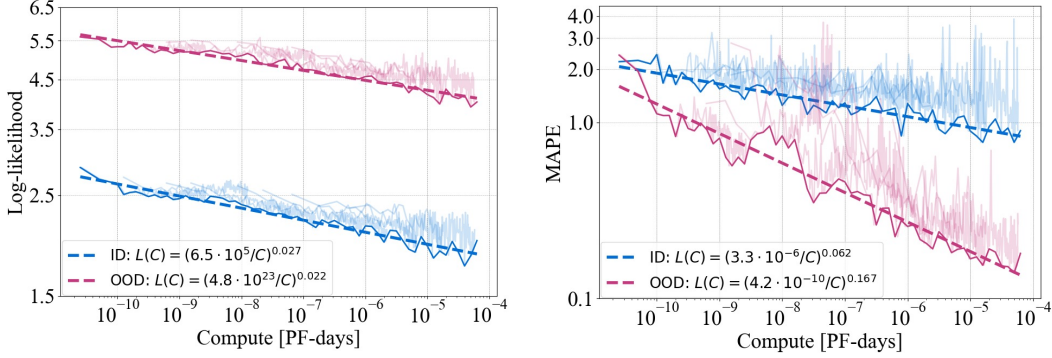


Figure 3: **Compute Scaling.** The computation scaling results show that model performance approximately follows a power law trend with increasing compute, consistent across both ID and OOD scenarios. The ID and OOD results demonstrate that a lower bound exists for the loss and MAPE under a given computational budget.

$$L(N) \approx \left( \frac{N_c}{N} \right)^{\alpha_N}, \quad (2)$$

where  $L$  is the performance metric function (i.e., MAPE, or log-likelihood),  $N$  is a given parameter count,  $N_c$  is the normalization coefficient, and  $\alpha_N$  is the exponent value that indicates the degree of performance improvement expected as we scale up  $N$ .

Observing the log-likelihood metric, the lines fitting the scaling laws for both ID and OOD data exhibits a roughly constant shift and close slopes. This implies that while models incur a consistent performance bias when transferred to OOD data, their scaling patterns correlate well with their performance on the ID data. When evaluated using MAPE, the power-law for OOD scenario shows a bigger exponent value than ID scenario. This indicates that increasing model size yields greater improvements in OOD performance than ID performance. In other words, for models with weak OOD generalization capabilities, increasing model size may enable them to perform equally well on both ID and OOD data.

**Compute Scaling.** Following the similar method in (Kaplan et al., 2020), we estimate the compute budget using the formula  $C = 6NBS$ , where  $B$  is the batch size,  $S$  is the number of parameter updates, i.e. the input sequence length, and 6 is the factor to account for the forward and backward passes. The ID and OOD test loss for compute budget varying over six orders of magnitude are

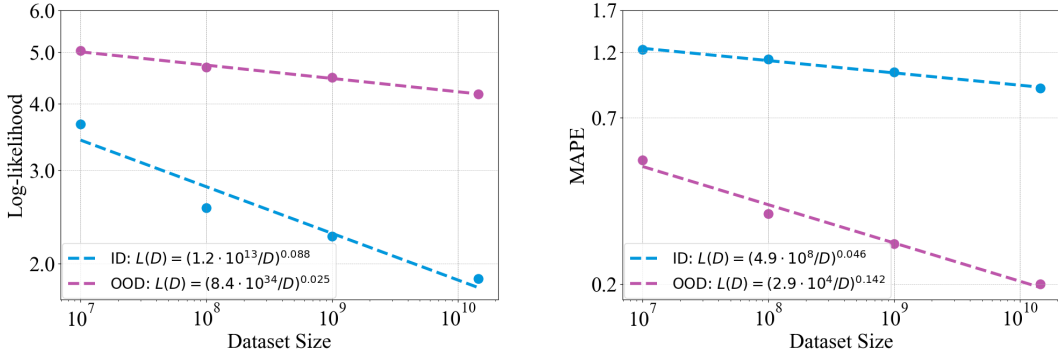


Figure 4: **Data Scaling.** The blue and red plots illustrate how data volume affects the **ID** and **OOD** forecasting performance of encoder-only Transformers, evaluated using log-likelihood and MAPE metrics. The results indicate that in both scenarios, model performance scales approximately as a power law with increasing data volume.

shown in Fig 3. We see that the optimal results for each compute budget are achieved by different model sizes  $N$ , but the lowest loss decreases according to an approximate power law with respect to the amount of training compute. The lowest losses appear as the heavy lines, which can be fit with

$$L(C) \approx \left(\frac{C_c}{C}\right)^{\alpha_C}. \quad (3)$$

We observed significant noise in log-likelihood and MAPE during training, which may be caused by the learning rate scheduler and the random sampling evaluation strategy. Similar to parameter scaling, the ID and OOD log-likelihood shows similar scaling patterns; however, when evaluated using MAPE, the OOD power law shows larger exponent values than the ID power law.

**Data Scaling.** We display empirical trends for the performance as function of dataset size  $D$  in Fig 4. For the trend, we trained multiple 1B encoder-only Transformers on a series of subsets of the 15B pre-training dataset and report the averaged evaluation results during training. We see that the log-likelihood and MAPE can be fit well with simple power-law

$$L(D) \approx \left(\frac{D_c}{D}\right)^{\alpha_D}. \quad (4)$$

Different from the parameter scaling and computational scaling, we found that when evaluated using log-likelihood, ID and OOD performance do not exhibit the same scaling behavior. Instead, ID performance is more sensitive to the scaling of dataset size compared to OOD performance. However, similar to the observations on the other two factors, the impact of data scaling on MAPE in OOD data is greater than its impact on MAPE in ID data. This suggests that the scaling of various factors yields greater improvements in OOD performance than ID performance.

**Cross-Distribution Scaling Effects Summary.** We summarize the key findings on how model ID and OOD performance scales with the model parameters, data volume, and compute. (1) In both ID and OOD univariate time series forecasting, model performance follows a simple power law as a function of model parameters, data volume, and compute. (2) For log-likelihood loss, the model exhibits similar scaling patterns in both ID and OOD scenarios, in terms of model size or compute resources. (3) When using MAPE as the metric, scaling of all three factors results in greater improvements in OOD performance compared to ID performance.

### 3.2 SCALING LAWS ACROSS MODEL ARCHITECTURES

The above results suggest that the power-law captures the scaling behavior of the encoder-only Transformer in both ID and OOD scenarios. Similarly, we analyze the scaling properties of the decoder-only Transformer, along with two other state-of-the-art TSFMs, Chronos and Moirai, to assess the impact of model architectures on scaling behavior.

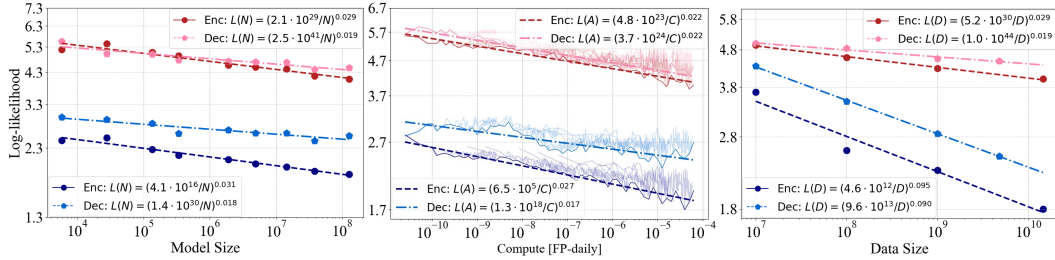


Figure 5: **Scaling Laws of Encoder-only vs. Decoder-only Transformer.** This figure presents a comparison of scaling behaviors on log-likelihood between encoder-only and decoder-only Transformer across three different axes: number of parameters, compute, and dataset size. Overall, encoder-only Transformer shows better scalability on model parameters, computation and dataset sizes across ID and OOD data.

**Encoder-only vs. Decoder-only Transformer.** Fig. 5 presents a comparison of the scaling patterns between encoder-only and decoder-only Transformers. In terms of parameter scaling, the power law exponent of the encoder-only Transformer is consistently higher than that of the decoder-only Transformer across ID and OOD settings, indicating its superior scalability on parameters. Moreover, for a given number of parameters, the encoder-only Transformer generally achieves a lower log-likelihood loss, signifying better forecasting performance. Regarding compute scaling, both models demonstrate highly similar compute scalability on OOD data and slightly differ on ID data. When it comes to data, the scaling law fitting lines for encoder-only and decoder-only Transformers exhibit nearly constant offsets and similar slopes on data size scaling. This suggests that despite differences in performance, the scaling behavior of encoder-only and decoder-only Transformers is highly similar on pre-training dataset size.

**Encoder-only Transformer vs. Moirai.** Moirai is a TSFM based on an encoder-only Transformer architecture. It introduces any-variate attention to capture relationships between multiple variables. Additionally, Moirai incorporates a multi-scale patch embedding to handle different frequency patterns, and a more diverse mixture distribution to model real-world probability distributions. Fig. 6 shows a comparison between the scaling behavior of encoder-only Transformer and Moirai. On ID data, Moirai demonstrates better performance. However, for OOD data, as the number of model parameters increases, Moirai is gradually surpassed by the encoder-only Transformer. Comparing the power-law lines of the two models, we see that Moirai shows a smaller slope, indicating relatively weaker scalability. Collectively, Moirai shows significant improvements on ID time series forecast than our baseline, but some designs may limit its scalability on OOD data.

**Decoder-only Transformer vs. Chronos.** Chronos-T5 is an encoder-decoder Transformer-based TSFM that, like decoder-only Transformers, follows an auto-regressive prediction approach but uses a separate encoder to extract contextual information. It adopts point-wise prediction and transform numerical regression into discrete probability prediction. Fig. 7 compares the scaling patterns of decoder-only Transformers and Chronos-T5. When evaluated with log-likelihood, Chronos-T5 exhibits power laws with very small exponents, indicating limited scalability. We attribute this to the discrete probability prediction, as log-likelihood loss on a discrete distribution is not distance-sensitive, meaning the loss remains high unless the predicted value exactly matches the label. Compared to log-likelihood, symmetric mean absolute percentage error (SMAPE, definition is shown in Appendix C.3) is a more appropriate metric for evaluating the two models. Chronos-T5 shows a slight advantage in performance and scalability on ID data. However, on OOD data, the decoder-only Transformer performs much better. Despite some performance differences, both models exhibit similar scaling patterns on OOD data. Overall, the design improvements in Chronos-T5 enhance ID time series forecasting, but they do not effectively improve OOD generalization.

**Cross-Architecture Scaling Effects Summary.** Our analysis of the scaling properties across architectures reveals several key findings: (1) Model architecture and design play a crucial role in determining scalability. (2) Encoder-only models demonstrate superior scalability and performance compared to decoder-only models, although both architectures exhibit similar scaling trends. (3)



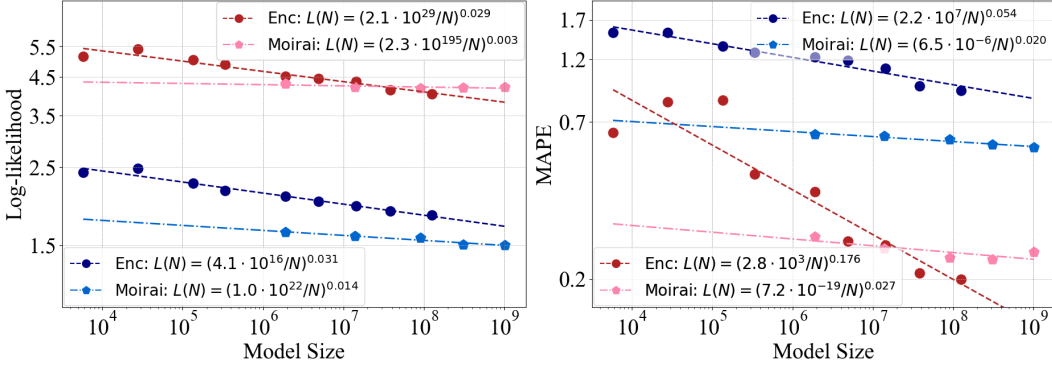


Figure 6: **Scaling Laws of Encoder-only Transformer vs. Moirai.** This figure compares parameter scaling between the encoder-only Transformer and Moirai. While Moirai demonstrates notable improvements on **ID** test data compared to the baseline, certain design choices may hinder its scalability on **OOD** data.

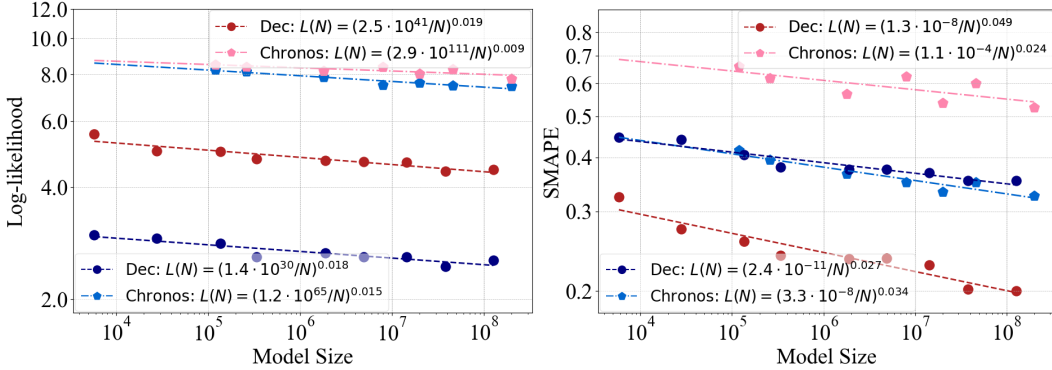


Figure 7: **Scaling Laws of Decoder-only Transformer vs. Chronos.** This figure presents a comparison of parameter scaling between decoder-only Transformer and Chronos. The design introduced by Chronos enhances **ID** time series forecasting, but fails to improve the generalization of **OOD**.

While Chronos and Moirai improve in-distribution **ID** forecasting, these gains do **not** extend effectively to **OOD** scenarios.

#### 4 DESIGN PRINCIPLES FOR TIME SERIES FOUNDATION MODELS

Building on our findings regarding the scaling laws in TSFMs, we elaborate design principles to guide the development of effective and scalable models. These principles are framed around three key dimensions: training data, model parameters and architecture, as well as computational budget.

**Training Data.** Our experiments show that increasing the size of the training dataset leads to a greater performance improvement on **OOD** data compared to **ID** data. Enlarging the pre-training dataset is crucial for achieving better generalization. However, maintaining diversity within the dataset is equally important while increasing the data volume. Additionally, we observed that while there is a performance bias between encoder-only and decoder-only Transformers, they exhibit a consistent scaling pattern as the data size increases. This indicates that the benefits of data expansion are not influenced by model architecture, meaning that collecting more data can proceed in parallel with model improvements.

**Model Parameters and Architecture.** Our study highlights that model size is the most critical factor for improving TSFM performance. Among the three factors we examined, increasing the model size yielded the greatest benefit for **ID** forecast. In terms of architecture, an encoder-only Trans-



former architecture generally performs better and is more scalable than a decoder-only Transformer. Additionally, although the advanced models Chronos and Moirai showed some improvements in ID time series forecast, they failed to enhance OOD prediction capabilities. We speculate this is due to inductive biases introduced by the model modifications that do not generalize well. Compared to our baseline models, the scalability of Moirai and Chronos decreased, suggesting that the introduced designs limit the scalability of TSFMs. Model architecture significantly impacts scalability, and a good design should promote improvements in performance, generalization, and scalability.

**Computational Budget.** The power law we established indicates that there is an unbreakable lower bound for loss and MAPE under a given computational budget. This means that, with other factors remaining constant, as the model size increases, more compute resources must be invested to achieve better performance. However, different training objectives or model architectures can significantly affect this bound. For example, using masked recovery as a training objective typically shows a lower bound compared to next-token prediction. Similar to the scaling behavior of model size and dataset size, the increase in compute scale has a greater impact on improving OOD performance than on ID performance. This suggests that achieving robust generalization across distributions requires larger models, more data, and greater compute resources.

## 5 RELATED WORKS

**Neural Scaling Laws.** Neural scaling laws seek to provide a predictive framework for optimizing the allocation of computational resources to maximize model performance. In language domains, Kaplan et al. (2020) demonstrated that performance follows a power-law relationship, improving as more computational resources, parameters, and data are utilized. Subsequent research has expanded this to predict other factors, such as downstream task performance (Isik et al., 2024) and inference time (Sardana et al., 2024). In vision domains, scaling laws have been explored in areas like discriminative modeling (Hestness et al., 2017) and visual auto-regressive modeling (Henighan et al., 2020). Recently, Edwards et al. (2024) introduced scaling laws for large time series models, showing that performance scales according to a power law with model size, compute, and dataset size. Shi et al. (2024a) examined the effect of time-series forecasting horizon on model scaling behavior, offering a theoretical framework to explain its influence. However, both studies have focused on in-distribution scenarios, leaving the investigation of scaling laws in out-of-distribution contexts largely unexplored.

**Time Series Foundation Models.** Foundation models (Das et al., 2024; Goswami et al., 2024) represent a new paradigm aimed at generalizing across diverse domains and tasks by leveraging knowledge from large-scale data in the pre-training phase. They have significantly advanced time series forecasting, particularly in zero-shot scenarios, where predictions are made on data from previously unseen domains. For instance, Woo et al. (2024) introduced Moirai, an encoder-only transformer architecture that employs an “any-variate” attention mechanism to capture dependencies in multivariate time series. Ansari et al. (2024) proposed a method that tokenizes time series values through scaling and quantization into a fixed vocabulary, training a series of transformer-based models known as Chronos. Liu et al. (2024) developed Timer, a simple decoder-only transformer architecture designed for univariate time series forecasting, while Rasul et al. (2023) introduced Lag-Llama, a decoder-only transformer that integrates lags as covariates to improve forecasting accuracy. These models incorporate various modifications to the standard Transformer architecture for time series data. However, the impact of these changes on model scaling properties has not been systematically studied. As model size increases, it remains an open question whether these modifications will continue to enhance performance.

## 6 DISCUSSION

### 6.1 ADDITIONAL STUDIES

We also conduct the following analysis to better understand the scaling behaviors of TSFMs. Due to the space limit, see their details in Appendix D.2 to D.4 .

**Emergent Behaviors.** Fig. 8 shows some examples of zero-shot OOD time series forecasting, where the model’s performance remains low until the model size reaches a critical threshold, after

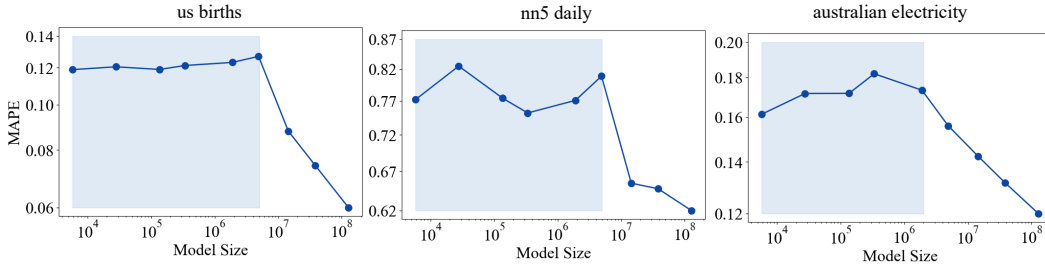


Figure 8: Case studies on the “emergent abilities” of scaling time series model: We present three examples of zero-shot (**unseen**) out-of-distribution (OOD) time series prediction. In the US births, NN5 daily, and Australian electricity datasets, we observed that model behavior deviates from expected power law patterns, instead exhibiting characteristics more akin to *emergent phenomena*.

which performance improves significantly. This scaling behavior deviates from the previously observed power law and is more akin to emergent phenomena (Wei et al., 2022). This suggests that achieving good forecasting performance for certain time series may require a model with sufficient parameters to capture the underlying dynamic systems. For example, if a system of multistep differential equations requires  $l$  sequential computation steps, the model may require a depth of at least  $O(l)$  layers to handle the complexity.

**Sample Efficiency.** Appendix D.2, Fig 9 shows the evaluation results during training. Large models are more sample-efficient than small models, reaching the better performance with the same optimization steps and using fewer time points.

**Scaling Pattern Depends on Data Distributions.** Appendix D.3, Fig. 10 shows the scaling behavior of TSFMs on Monash dataset, suggesting that OOD scaling behaviors depend on the relationship between the unseen data distribution and the training data distribution.

**Scaling Pattern Depends on Performance Metrics.** Appendix C.3, Fig. 11; 12;13 show the scaling behavior of continuous ranked probability score (CRPS), symmetric mean absolute percentage error (sMAPE), and mean absolute error (MAE). Comparing the results with log-likelihood and MAPE, we see obvious difference in the scaling patterns.

## 6.2 CONCLUSION

We have observed consistent scaling of encoder-only Transformer log-likelihood loss with parameter count, training computation and dataset size on both ID and OOD test data, as encapsulated in a power law. The experimental results show that as the number of parameters, computational resources, and training data increase, both models’ ID and OOD performance will continue to improve. Furthermore, our established laws suggest that for ID forecasting performance, larger model may be more important than more data. While, larger training dataset size plays a more crucial role in improving OOD forecasting performance.

We have also study the scaling properties of two common types of TSFMs, encoder-only Transformer and decoder-only Transformer. The two architectures show different scaling patterns in model size, computational resources, and training data. Generally, encoder-only Transformers show better performance and scalability. Moreover, we further include two advanced TSFMs, Chronos and Moirai, as specific cases to study the impact of model design on scaling behavior. We find that both Chronos and Moirai improve ID forecasting performance, but these gains can not translate effectively to OOD scenarios.

Our experiments independently investigated the scaling behavior of TSFMs in terms of parameter count, computational resources, and training data size, assuming other factors were unlimited. In future work, it would be valuable to develop a unified model to explore the relationships between these factors. This could help guide the community in optimizing resource allocation when one resource is limited. Additionally, multiple studies have shown that model performance varies across different context window lengths and forecast horizons. In future research, we plan to incorporate the impact of context length and forecast horizon on scalability.

## REFERENCES

- Alexander Alexandrov, Konstantinos Benidis, Michael Bohlke-Schneider, Valentin Flunkert, Jan Gasthaus, Tim Januschowski, Danielle C. Maddix, Syama Sundar Rangapuram, David Salinas, Jasper Schulz, Lorenzo Stella, Ali Caner Türkmen, and Bernie Wang. Gluonts: Probabilistic and neural time series modeling in python. *J. Mach. Learn. Res.*, 21:116:1–116:6, 2020. URL <https://api.semanticscholar.org/CorpusID:226717462>.
- Abdul Fatir Ansari, Lorenzo Stella, Caner Turkmen, Xiyuan Zhang, Pedro Mercado, Huibin Shen, Oleksandr Shchur, Syama Sundar Rangapuram, Sebastian Pineda Arango, Shubham Kapoor, Jasper Zschiegner, Danielle C. Maddix, Michael W. Mahoney, Kari Torkkola, Andrew Gordon Wilson, Michael Bohlke-Schneider, and Yuyang Wang. Chronos: Learning the language of time series. *ArXiv*, abs/2403.07815, 2024. URL <https://api.semanticscholar.org/CorpusID:268363551>.
- Abhimanyu Das, Weihao Kong, Rajat Sen, and Yichen Zhou. A decoder-only foundation model for time-series forecasting. In *Forty-first International Conference on Machine Learning, ICML 2024, Vienna, Austria, July 21-27, 2024*. OpenReview.net, 2024. URL <https://openreview.net/forum?id=jn2iTJas6h>.
- Hoang Anh Dau, A. Bagnall, Kaveh Kamgar, Chin-Chia Michael Yeh, Yan Zhu, Shaghayegh Gharghabi, Chotirat Ann Ratanamahatana, and Eamonn J. Keogh. The ucr time series archive. *IEEE/CAA Journal of Automatica Sinica*, 6:1293–1305, 2018. URL <https://api.semanticscholar.org/CorpusID:53019704>.
- Alexey Dosovitskiy, Lucas Beyer, Alexander Kolesnikov, Dirk Weissenborn, Xiaohua Zhai, Thomas Unterthiner, Mostafa Dehghani, Matthias Minderer, Georg Heigold, Sylvain Gelly, Jakob Uszkoreit, and Neil Houlsby. An image is worth 16x16 words: Transformers for image recognition at scale. *ArXiv*, abs/2010.11929, 2020. URL <https://api.semanticscholar.org/CorpusID:225039882>.
- Thomas D. P. Edwards, James Alvey, Justin Alsing, Nam H. Nguyen, and Benjamin D. Wandelt. Scaling-laws for large time-series models. *ArXiv*, abs/2405.13867, 2024. URL <https://api.semanticscholar.org/CorpusID:269982332>.
- Patrick Emami, Abhijeet Sahu, and Peter Graf. Buildingsbench: A large-scale dataset of 900k buildings and benchmark for short-term load forecasting. In Alice Oh, Tristan Naumann, Amir Globerson, Kate Saenko, Moritz Hardt, and Sergey Levine (eds.), *Advances in Neural Information Processing Systems 36: Annual Conference on Neural Information Processing Systems 2023, NeurIPS 2023, New Orleans, LA, USA, December 10 - 16, 2023*, 2023. URL [http://papers.nips.cc/paper\\_files/paper/2023/hash/3f17bf868966df01ca125e5bbc9ee24e-Abstract-Datasets\\_and\\_Benchmarks.html](http://papers.nips.cc/paper_files/paper/2023/hash/3f17bf868966df01ca125e5bbc9ee24e-Abstract-Datasets_and_Benchmarks.html).
- Wei Fan, Pengyang Wang, Dongkun Wang, Dongjie Wang, Yuanchun Zhou, and Yanjie Fu. Dish-ts: A general paradigm for alleviating distribution shift in time series forecasting. In *AAAI Conference on Artificial Intelligence*, 2023. URL <https://api.semanticscholar.org/CorpusID:257232506>.
- Valentin Flunkert, David Salinas, and Jan Gasthaus. Deepar: Probabilistic forecasting with autoregressive recurrent networks. *ArXiv*, abs/1704.04110, 2017. URL <https://api.semanticscholar.org/CorpusID:12199225>.
- B. Ghorbani, Orhan Firat, Markus Freitag, Ankur Bapna, Maxim Krikun, Xavier García, Ciprian Chelba, and Colin Cherry. Scaling laws for neural machine translation. *ArXiv*, abs/2109.07740, 2021. URL <https://api.semanticscholar.org/CorpusID:237532682>.
- Rakshitha Godahewa, C. Bergmeir, Geoffrey I. Webb, Rob J Hyndman, and Pablo Montero-Manso. Monash time series forecasting archive. *ArXiv*, abs/2105.06643, 2021. URL <https://api.semanticscholar.org/CorpusID:234681550>.

- Mononito Goswami, Konrad Szafer, Arjun Choudhry, Yifu Cai, Shuo Li, and Artur Dubrawski. Moment: A family of open time-series foundation models. *ArXiv*, abs/2402.03885, 2024. URL <https://api.semanticscholar.org/CorpusID:267500205>.
- Tom Henighan, Jared Kaplan, Mor Katz, Mark Chen, Christopher Hesse, Jacob Jackson, Heewoo Jun, Tom B. Brown, Prafulla Dhariwal, Scott Gray, Chris Hallacy, Benjamin Mann, Alec Radford, Aditya Ramesh, Nick Ryder, Daniel M. Ziegler, John Schulman, Dario Amodei, and Sam McCandlish. Scaling laws for autoregressive generative modeling. *ArXiv*, abs/2010.14701, 2020. URL <https://api.semanticscholar.org/CorpusID:225094178>.
- Joel Hestness, Sharan Narang, Newsha Ardalani, Gregory Frederick Diamos, Heewoo Jun, Hassan Kianinejad, Md. Mostofa Ali Patwary, Yang Yang, and Yanqi Zhou. Deep learning scaling is predictable, empirically. *ArXiv*, abs/1712.00409, 2017. URL <https://api.semanticscholar.org/CorpusID:2222076>.
- Rob J Hyndman and George Athanasopoulos. Forecasting: principles and practice. 2013. URL <https://api.semanticscholar.org/CorpusID:215822294>.
- Berivan Isik, Natalia Ponomareva, Hussein Hazimeh, Dimitris Paparas, Sergei Vassilvitskii, and Sanmi Koyejo. Scaling laws for downstream task performance of large language models. *ArXiv*, abs/2402.04177, 2024. URL <https://api.semanticscholar.org/CorpusID:267499809>.
- Jiawei Jiang, Chengkai Han, Wenjun Jiang, Wayne Xin Zhao, and Jingyuan Wang. Libcity: A unified library towards efficient and comprehensive urban spatial-temporal prediction. 2023. URL <https://api.semanticscholar.org/CorpusID:258352728>.
- Ming Jin, Qingsong Wen, Yuxuan Liang, Chaoli Zhang, Siqiao Xue, Xue Wang, James Zhang, Yi Wang, Haifeng Chen, Xiaoli Li, et al. Large models for time series and spatio-temporal data: A survey and outlook. *arXiv preprint arXiv:2310.10196*, 2023.
- Jared Kaplan, Sam McCandlish, Tom Henighan, Tom B. Brown, Benjamin Chess, Rewon Child, Scott Gray, Alec Radford, Jeff Wu, and Dario Amodei. Scaling laws for neural language models. *ArXiv*, abs/2001.08361, 2020. URL <https://api.semanticscholar.org/CorpusID:210861095>.
- Xu Liu, Yutong Xia, Yuxuan Liang, Junfeng Hu, Yiwei Wang, Lei Bai, Chao Huang, Zhenguang Liu, Bryan Hooi, and Roger Zimmermann. Largest: A benchmark dataset for large-scale traffic forecasting. In Alice Oh, Tristan Naumann, Amir Globerson, Kate Saenko, Moritz Hardt, and Sergey Levine (eds.), *Advances in Neural Information Processing Systems 36: Annual Conference on Neural Information Processing Systems 2023, NeurIPS 2023, New Orleans, LA, USA, December 10 - 16, 2023*, 2023. URL [http://papers.nips.cc/paper\\_files/paper/2023/hash/ee57cd73a76bd927ffca3dda1dc3b9d4-Abstract-Datasets\\_and\\_Benchmarks.html](http://papers.nips.cc/paper_files/paper/2023/hash/ee57cd73a76bd927ffca3dda1dc3b9d4-Abstract-Datasets_and_Benchmarks.html).
- Yong Liu, Haoran Zhang, Chenyu Li, Xiangdong Huang, Jianmin Wang, and Mingsheng Long. Timer: Generative pre-trained transformers are large time series models. In *International Conference on Machine Learning*, 2024. URL <https://api.semanticscholar.org/CorpusID:267412273>.
- James E Matheson and Robert L Winkler. Scoring rules for continuous probability distributions. *Management science*, 22(10):1087–1096, 1976.
- Tung Nguyen, Jason Jewik, Hritik Bansal, Prakhar Sharma, and Aditya Grover. Climate-learn: Benchmarking machine learning for weather and climate modeling. In Alice Oh, Tristan Naumann, Amir Globerson, Kate Saenko, Moritz Hardt, and Sergey Levine (eds.), *Advances in Neural Information Processing Systems 36: Annual Conference on Neural Information Processing Systems 2023, NeurIPS 2023, New Orleans, LA, USA, December 10 - 16, 2023*, 2023. URL [http://papers.nips.cc/paper\\_files/paper/2023/hash/ed73c36e771881b232ef35fa3aldec14-Abstract-Datasets\\_and\\_Benchmarks.html](http://papers.nips.cc/paper_files/paper/2023/hash/ed73c36e771881b232ef35fa3aldec14-Abstract-Datasets_and_Benchmarks.html).

- Yuqi Nie, Nam H. Nguyen, Phanwadee Sinthong, and Jayant Kalagnanam. A time series is worth 64 words: Long-term forecasting with transformers. In *The Eleventh International Conference on Learning Representations, ICLR 2023, Kigali, Rwanda, May 1-5, 2023*. OpenReview.net, 2023. URL <https://openreview.net/forum?id=Jbdc0vTOcol>.
- Yuqi Nie, Yaxuan Kong, Xiaowen Dong, John M Mulvey, H Vincent Poor, Qingsong Wen, and Stefan Zohren. A survey of large language models for financial applications: Progress, prospects and challenges. *arXiv preprint arXiv:2406.11903*, 2024.
- Youngsuk Park, Danielle Maddix, François-Xavier Aubet, Kelvin Kan, Jan Gasthaus, and Yuyang Wang. Learning quantile functions without quantile crossing for distribution-free time series forecasting. In *International Conference on Artificial Intelligence and Statistics*, pp. 8127–8150. PMLR, 2022.
- Raquel Prado. Bayesian forecasting and dynamic models. 2020. URL <https://api.semanticscholar.org/CorpusID:121876157>.
- Colin Raffel, Noam Shazeer, Adam Roberts, Katherine Lee, Sharan Narang, Michael Matena, Yanqi Zhou, Wei Li, and Peter J Liu. Exploring the limits of transfer learning with a unified text-to-text transformer. *Journal of machine learning research*, 21(140):1–67, 2020.
- Kashif Rasul, Arjun Ashok, Andrew Robert Williams, Arian Khorasani, George Adamopoulos, Rishika Bhagwatkar, Marin Bilos, Hena Ghonia, Nadhir Vincent Hassen, Anderson Schneider, Sahil Garg, Alexandre Drouin, Nicolas Chapados, Yuriy Nevmyvaka, and Irina Rish. Lag-llama: Towards foundation models for time series forecasting. *ArXiv*, abs/2310.08278, 2023. URL <https://api.semanticscholar.org/CorpusID:269766909>.
- Nikhil Sardana, Jacob Portes, Sasha Doubov, and Jonathan Frankle. Beyond chinchilla-optimal: Accounting for inference in language model scaling laws. In *Forty-first International Conference on Machine Learning, ICML 2024, Vienna, Austria, July 21-27, 2024*. OpenReview.net, 2024. URL <https://openreview.net/forum?id=0bmXrtTDUu>.
- Jingzhe Shi, Qinwei Ma, Huan Ma, and Lei Li. Scaling law for time series forecasting. *ArXiv*, abs/2405.15124, 2024a. URL <https://api.semanticscholar.org/CorpusID:270045141>.
- Xiaoming Shi, Shiyu Wang, Yuqi Nie, Dianqi Li, Zhou Ye, Qingsong Wen, and Ming Jin. Time-moe: Billion-scale time series foundation models with mixture of experts. *arXiv preprint arXiv:2409.16040*, 2024b.
- Jianlin Su, Murtadha H. M. Ahmed, Yu Lu, Shengfeng Pan, Wen Bo, and Yunfeng Liu. Roformer: Enhanced transformer with rotary position embedding. *Neurocomputing*, 568:127063, 2024. doi: 10.1016/J.NEUCOM.2023.127063. URL <https://doi.org/10.1016/j.neucom.2023.127063>.
- Chang Wei Tan, Christoph Bergmeir, François Petitjean, and Geoffrey I Webb. Time series extrinsic regression: Predicting numeric values from time series data. *Data Mining and Knowledge Discovery*, 35(3):1032–1060, 2021.
- Yihe Wang, Yu Han, Haishuai Wang, and Xiang Zhang. Contrast everything: A hierarchical contrastive framework for medical time-series. In Alice Oh, Tristan Naumann, Amir Globerson, Kate Saenko, Moritz Hardt, and Sergey Levine (eds.), *Advances in Neural Information Processing Systems 36: Annual Conference on Neural Information Processing Systems 2023, NeurIPS 2023, New Orleans, LA, USA, December 10 - 16, 2023*, 2023a. URL [http://papers.nips.cc/paper\\_files/paper/2023/hash/ae7d9c77b5ff9e3b7833a68523b880f2-Abstract-Conference.html](http://papers.nips.cc/paper_files/paper/2023/hash/ae7d9c77b5ff9e3b7833a68523b880f2-Abstract-Conference.html).
- Yuxuan Wang, Haixu Wu, Jiayang Dong, Yong Liu, Mingsheng Long, and Jianmin Wang. Deep time series models: A comprehensive survey and benchmark. *ArXiv*, abs/2407.13278, 2024. URL <https://api.semanticscholar.org/CorpusID:271270683>.
- Zhixian Wang, Qingsong Wen, Chaoli Zhang, Liang Sun, Leandro Von Krannichfeldt, and Yi Wang. Benchmarks and custom package for electrical load forecasting. *ArXiv*, abs/2307.07191, 2023b. URL <https://api.semanticscholar.org/CorpusID:259924876>.

- Jason Wei, Yi Tay, Rishi Bommasani, Colin Raffel, Barret Zoph, Sebastian Borgeaud, Dani Yogatama, Maarten Bosma, Denny Zhou, Donald Metzler, Ed Hui hsin Chi, Tatsunori Hashimoto, Oriol Vinyals, Percy Liang, Jeff Dean, and William Fedus. Emergent abilities of large language models. *ArXiv*, abs/2206.07682, 2022. URL <https://api.semanticscholar.org/CorpusID:249674500>.
- Haomin Wen, Youfang Lin, Lixia Wu, Xiaowei Mao, Tianyue Cai, Yunfeng Hou, Shengnan Guo, Yuxuan Liang, Guangyin Jin, Yiji Zhao, et al. A survey on service route and time prediction in instant delivery: Taxonomy, progress, and prospects. *IEEE Transactions on Knowledge and Data Engineering*, 2024.
- Qingsong Wen, Tian Zhou, Chao Zhang, Weiqiu Chen, Ziqing Ma, Junchi Yan, and Liang Sun. Transformers in time series: A survey. In *International Joint Conference on Artificial Intelligence*, 2022. URL <https://api.semanticscholar.org/CorpusID:246863823>.
- Gerald Woo, Chenghao Liu, Akshat Kumar, and Doyen Sahoo. Pushing the limits of pre-training for time series forecasting in the cloudops domain. *ArXiv*, abs/2310.05063, 2023. URL <https://api.semanticscholar.org/CorpusID:263831258>.
- Gerald Woo, Chenghao Liu, Akshat Kumar, Caiming Xiong, Silvio Savarese, and Doyen Sahoo. Unified training of universal time series forecasting transformers. In *Forty-first International Conference on Machine Learning, ICML 2024, Vienna, Austria, July 21-27, 2024*. OpenReview.net, 2024. URL <https://openreview.net/forum?id=Yd8eHMY1wz>.
- Haixu Wu, Tengge Hu, Yong Liu, Hang Zhou, Jianmin Wang, and Mingsheng Long. Timesnet: Temporal 2d-variation modeling for general time series analysis. In *The Eleventh International Conference on Learning Representations, ICLR 2023, Kigali, Rwanda, May 1-5, 2023*. OpenReview.net, 2023. URL [https://openreview.net/forum?id=ju\\_Uqw3840q](https://openreview.net/forum?id=ju_Uqw3840q).
- Chao-Han Huck Yang, Yun-Yun Tsai, and Pin-Yu Chen. Voice2series: Reprogramming acoustic models for time series classification. In *International conference on machine learning*, pp. 11808–11819. PMLR, 2021.
- Kexin Zhang, Qingsong Wen, Chaoli Zhang, Rongyao Cai, Ming Jin, Yong Liu, James Zhang, Y. Liang, Guansong Pang, Dongjin Song, and Shirui Pan. Self-supervised learning for time series analysis: Taxonomy, progress, and prospects. *IEEE Transactions on Pattern Analysis and Machine Intelligence*, 46:6775–6794, 2023. URL <https://api.semanticscholar.org/CorpusID:259203853>.

## A APPENDIX: DATASETS AND SETUP INFORMATION

Previous work has proposed several public large-scale time series datasets, e.g. LOTSA (Woo et al., 2024) and UTSD (Liu et al., 2024). Instead of using these datasets directly, we built a pre-training corpus through data filtering. There are three main reasons for this: First, these datasets contain numerous periodic time series with substantial pattern redundancy. Second, these datasets show a heavily long-tailed distribution, with multiple domains accounting for less than 5% of the total. Third, data quality is variable, with some time series missing many observations or having low signal-to-noise ratios. To address these issues, we developed a data filtering pipeline:

**Deduplication.** In these public datasets, we observed significant redundancy across many subsets. This redundancy typically manifests as numerous repeated patterns within individual samples or high similarity between multiple samples. Such redundancy can negatively impact training efficiency. To address this issue, we applied a down-sampling strategy for datasets with redundant samples based on the data sampling period.

**Quality Filtering.** We focused on selecting time series data that have no missing values and a signal-to-noise ratio (SNR) greater than 20 dB to ensure better predictability. To calculate the SNR, we first used Fourier transform to identify the low-frequency components of the time series. We then applied a low-pass Butterworth filter to extract these low-frequency components as the signal, with the remaining residuals considered as noise.

**Domain Balancing.** In the Lotsa dataset, the climate domain accounts for nearly 90% of the data, while the remaining seven domains collectively represent only 10%. To create a more balanced pre-training dataset, we selected the traffic domain, which contains 4.8 billion time points, as the reference. We then scaled the data from the other domains to a similar magnitude.

Following the aforementioned processing steps, we compiled a high-quality time series dataset containing a total of 14.46 billion time points across 7 domains. The data volume is sufficient to support training models with parameters ranging from  $10^3$  to  $10^8$  parameters. Furthermore, each domain includes at least 100 million time points, ensuring that even when the dataset is divided into subsets of various sizes, domain diversity is preserved. Below, we introduce the datasets for each domain and outline the key properties of the datasets after processing, including domain type, sampling frequency, number of time series, total number of observations, and data source.

**Climate.** The climate data are sourced primarily from the ERA5 and CMIP6 datasets, which provide time series for various climate-related variables, including temperature, humidity, and pressure levels. During data curation, we observed a high degree of similarity across yearly data. To reduce redundancy, only two years of data from ERA5 and CMIP6 were included.

**Energy.** The energy data primarily come from the BuildingsBench dataset, which provides time series data on residential and commercial building energy consumption. After applying quality filtering based on SNR, we selected samples from the Buildings-900K, BDG-2, and Sceaux datasets. Additionally, high-quality data from the ProEnFo library, including the GEF, ELF, PDB, Spanish, and Covid19\_Energy datasets, were incorporated.

**Transport.** The primary source for transport data is the LargeST traffic dataset, covering traffic flow in California from 2017 to 2021. We also integrated datasets from LibCity, PEMS, Loop Seattle, and Q-Traffic into our corpus.

**Cloud Operations.** The cloud operations data is from the large-scale CloudOps time series datasets, which measures various variables such as CPU and memory utilization.

**Healthcare.** We include a diverse sets of healthcare data from the ucr time series archive.

**Web.** The web data comprises the Kaggle Web Traffic Weekly dataset and the Wiki-Rolling dataset.

**Sales.** Here we use the Favorita Sales dataset.



Table 2: Pretraining datasets and key properties.

Dataset	Domain	Frequency	# Time Series	# Obs.	Source
CMIP6	Climate	6H	8192	2,870,476,800	Nguyen et al. (2023)
ERA5	Climate	H	8192	1,860,698,112	Nguyen et al. (2023)
Buildings900K	Energy	H	264980	2,321,489,780	Emami et al. (2023)
Australian Electricity	Energy	30T	5	1,153,584	Godahehwa et al. (2021)
BDG-2 Bear	Energy	H	91	1,482,312	Emami et al. (2023)
BDG-2 Fox	Energy	H	135	2,324,568	Emami et al. (2023)
BDG-2 Panther	Energy	H	136	893,840	Emami et al. (2023)
Sceaux	Energy	H	1	34,223	Emami et al. (2023)
Solar Power	Energy	4S	26	5,248	Godahehwa et al. (2021)
Covid19 Energy	Energy	H	1	31,912	Wang et al. (2023b)
Spanish	Energy	H	1	35,064	Wang et al. (2023b)
Elecdemand	Energy	30T	1	17,520	Godahehwa et al. (2021)
PDB	Energy	H	1	17,520	Wang et al. (2023b)
GEF17	Energy	H	8	140352	Wang et al. (2023b)
GEF14	Energy	H	1	17,520	Wang et al. (2023b)
ELF	Energy	H	1	21,792	Wang et al. (2023b)
Traffic Weekly	Transport	W	821	78,816	Godahehwa et al. (2021)
Q-Traffic	Transport	15T	45,148	257,200,384	Jiang et al. (2023)
PEMS04	Transport	5T	307	14,638,784	Jiang et al. (2023)
PEMS07	Transport	5T	883	23,789,760	Jiang et al. (2023)
PEMS08	Transport	5T	170	8,684,480	Jiang et al. (2023)
PEMS Bay	Transport	5T	325	15,975,920	Jiang et al. (2023)
Loop Seattle	Transport	5T	1,809	33,700,832	Jiang et al. (2023)
LargeST	Transport	5T	8521	4,452,510,528	Liu et al. (2023)
Azure VM Traces 2017	CloudOTS	5T	159,472	880,648,165	Woo et al. (2023)
Borg Cluster Data 2011	CloudOTS	5T	143,386	176,650,715	Woo et al. (2023)
Alibaba Cluster Trace 2018	CloudOTS	5T	58409	191,740,824	Woo et al. (2023)
Wiki-Rolling	Web	D	47,675	40,619,100	Alexandrov et al. (2020)
Kaggle Web Traffic Weekly	Web	W	145,063	15,206,232	Godahehwa et al. (2021)
Favorita Sales	Sales	D	111,840	139,111,860	Woo et al. (2024)
PigArtPressure	Health	-	312	624,000	Dau et al. (2018)
SelfRegulationSCP1	Health	0.004 SEC	3,366	3,015,936	Dau et al. (2018)
SelfRegulationSCP2	Health	0.004 SEC	2,660	3,064,320	Dau et al. (2018)
TDBrain	Health	0.002 SEC	28644	73,299,996	Wang et al. (2023a)
MotorImagery	Health	0.001 SEC	24,192	72,576,000	Dau et al. (2018)
PigCVP	Health	-	312	624,000	Dau et al. (2018)
AtrialFibrillation	Health	0.008 SEC	60	38,400	Dau et al. (2018)
IEEEPPG	Health	0.008 SEC	15,480	15,480,000	Tan et al. (2021)
BIDMC32HR	Health	-	15,898	63,592,000	Tan et al. (2021)

## B TIME SERIES MODELS

We define time series forecasting as the following problem: given a collection of multivariate time series samples with look back window  $L : (\mathbf{x}_1, \dots, \mathbf{x}_L)$  where each  $\mathbf{x}_t$  at time step  $t$  is a vector of dimension of  $M$ , our goal is to forecast  $T$  future values  $(\mathbf{x}_{L+1}, \dots, \mathbf{x}_{L+T})$ .

**Patch Embedding.** We split the input  $(\mathbf{x}_1, \dots, \mathbf{x}_L)$  into  $M$  univariate time series  $\mathbf{x}^{(i)} \in \mathbb{R}^{1 \times L}$ , independently forecasting future time series for each variate. Each univariate time series  $\mathbf{x}^{(i)}$  is first divided into non-overlapped patches. Specifically, given the patch length as  $P$ , the patching process will generate the a sequence of patches  $\mathbf{x}_p^{(i)} \in \mathbb{R}^{P \times N}$  where  $N = \lfloor \frac{L}{P} \rfloor$  is the number of patches. Then the patches are mapped to the latent space of  $d_m$  via a learnable linear projection  $\mathbf{W}_p \in \mathbb{R}^{d_m \times P}$ . In our baseline models, the patch size  $P$  is set to 32.

**Rotary Position Embedding.** Rotary Positional Embedding (RoPE) is a type of position encoding that encodes absolute positional information with a rotation matrix and naturally incorporates explicit relative position dependency in self-attention formulation. In detail, RoPE incorporates absolute position information to the embedding and transform them into queries, keys through function:

$$f_{q,k}(\mathbf{x}_m, m) = \mathbf{R}_{\Theta, m}^d \mathbf{W}_{q,k} \mathbf{x}_m$$

where

$$\mathbf{R}_{\Theta, m}^d = \begin{bmatrix} \mathbf{M}_1 & & & \\ & \mathbf{M}_2 & & \\ & & \ddots & \\ & & & \mathbf{M}_{d/2} \end{bmatrix}, \mathbf{M}_j = \begin{pmatrix} \cos m\theta_j & -\sin m\theta_j \\ \sin m\theta_j & \cos m\theta_j \end{pmatrix}$$

is the rotary matrix with pre-defined paramters  $\Theta = \{\theta_i = 10000^{-2(i-1)/d}, i \in [1, 2, \dots, d/2]\}$ ,  $\mathbf{W}_{q,k}$  is the learned query or key projection weights, and  $\mathbf{x}_m \in \mathbb{R}^d$  is the embedding of the  $m$  token. Next, applying RoPE to the dot product of query and key, we can obtain:

$$\mathbf{q}_m^\top \mathbf{k}_n = (\mathbf{R}_{\Theta, m}^d \mathbf{W}_q \mathbf{x}_m)^\top (\mathbf{R}_{\Theta, n}^d \mathbf{W}_k \mathbf{x}_n) = \mathbf{x}_m^\top \mathbf{W}_q \mathbf{R}_{\Theta, n-m}^d \mathbf{W}_k \mathbf{x}_n$$

where  $\mathbf{R}_{\Theta, n-m}^d = (\mathbf{R}_{\Theta, m}^d)^\top \mathbf{R}_{\Theta, n}^d$ . In this way, RoPE naturally incorporates relative position information through rotation matrix product. In general, the self-attention enhanced with RoPE can be written as

$$\text{Attention}(\mathbf{Q}, \mathbf{K}, \mathbf{V})_m = \frac{\sum_{n=1}^N (\mathbf{R}_{\Theta, m}^d \phi(\mathbf{q}_m))^\top (\mathbf{R}_{\Theta, n}^d \varphi(\mathbf{k}_n)) \mathbf{v}_n}{\sum_{n=1}^N \phi(\mathbf{q}_m)^\top \varphi(\mathbf{k}_n)}.$$

where  $\phi(\cdot), \varphi(\cdot)$  are usually non-negative functions, e.g.  $\text{elu}(\cdot)+1$ , or  $\exp(\cdot)$ . Overall, unlike the traditional approach of adding positional information before the query and key projection, RoPE utilizes a rotary matrix to transform query and key embeddings, effectively leveraging the geometric properties of vectors

**Mixture of Distributions.** As described in (Flunkert et al., 2017), our model predicts the parameters of a probability distribution, specifically a mixture of Student-t distributions. The probability density function for a random variable  $x$  following a Student-t distribution is given by:

$$p(x; \nu, \mu, \tau) = \frac{\Gamma(\frac{\nu+1}{2})}{\Gamma(\frac{\nu}{2}) \sqrt{\pi\nu\tau}} \left( 1 + \frac{1}{\nu} \left( \frac{x - \mu}{\tau} \right)^2 \right)^{-\frac{\nu+1}{2}}$$

with parameters  $\nu > 0, \mu \in \mathbb{R}, \tau > 0$  represent the degrees of freedom (df), location, and scale coefficient, respectively, and  $\Gamma$  is the gamma function. We modeled the predicted distribution using a mixture of four Student-t distributions. Our baseline model employs independent linear layers

to predict the distribution parameters: degrees of freedom, location, scale, and mixture weights. To ensure positive values for the scale and df, we apply a soft-plus transformation. The mixture weights are constrained within the probability simplex using a soft-max function. Additionally, to avoid undefined variance for low df values, we impose a lower bound of 2 on the df parameter

**Encoder-only Transformer.** The encoder-only Transformer has proven effective for time series tasks (Nie et al., 2023). In input time series, the future horizon is replaced by learnable mask tokens combined with position information. After passing through bidirectional attention blocks, the future representations are derived from these mask tokens and mapped to the parameters of a mixture distribution. Through sampling from the mixture distribution, we can get predictions for future patches. The pseudo code of encoder-only Transformer-based TSFM is as follows:

```
class EncoderOnlyTransformer(nn.Module):
    patch_tokenizer = nn.Linear(N, d_m)
    encoder = TransformerEncoder()
    mask_token_embedding = nn.Embedding(1, d_m)
    mixture_distribution_head = MixtureDistributionHead()

    def forecast(self, x, T):
        B, L, N = x.shape
        # Patch Embedding: (B, L, N) -> (B, L, d_m)
        x = patch_tokenizer(x)

        # Add mask tokens: (B, L, d_m) -> (B, L+T, d_m)
        mask_tokens = self.mask_token_embedding.weight.expand(B, T, -1)
        x = torch.cat((x, mask_tokens), dim=1)

        # Pass through bidirectional attention blocks
        encoded_output = self.encoder(x)

        # Truncate the future tokens: (B, L+T, d_m) -> (B, T, d_m)
        future_tokens = encoded_output[:, -self.num_mask_tokens:]

        # Predict the parameters of mixture distribution
        future_dist = self.mixture_distribution_head(future_tokens)

    return future_dist
```

**Decoder-only Transformer.** The key difference in the decoder-only Transformer is its unidirectional attention. In the input sequence, no masking is needed. The future horizon is predicted based on the preceding token. In other words, given a sequence of input patches, the model is optimized to predict the next patch as a function of all past patches. Similar to LLMs this can be done in parallel over the entire context window, and automatically enables the model to predict the future after having seen varying number of input patches. The pseudo code of decoder-only Transformer-based TSFM is as follows:

```
class DecoderOnlyTransformer(nn.Module):
    patch_tokenizer = nn.Linear(N, d_m)
    decoder = nn.TransformerDecoder()
    mixture_distribution_head = MixtureDistributionHead()

    def forecast(self, x, T):
        # Patch Embedding: (B, L, N) -> (B, L, d_m)
        x = self.patch_tokenizer(x)

        # Generate predictions for future time steps step-by-step
        preds = []

        for t in range(T):
            # If it's the first loop, use the original input
            tgt = torch.cat([x, *preds], dim=1) if preds else x
```

```

    # Pass through unidirectional attention blocks
    decoded_output = self.decoder(tgt)

    # Take the last token
    next_token = decoded_output[:, -1:, :]

    # Record the prediction of the current time step
    predictions.append(next_token)

    # Concatenate all predictions: (B, T, d_m)
    future_tokens = torch.cat(predictions, dim=1)

    # Predict the parameters of mixture distribution
    future_dist = self.mixture_distribution_head(future_tokens)

    return future_dist

```

## C IMPLEMENTATION DETAILS

### C.1 TRAINING SETUP

Based on the constructed datasets of different sizes, we trained a series of encoder-only Transformers and decoder-only Transformers with increasing data sizes and model parameters. To improve batch processing efficiency and handle varying sequence lengths, we employ sequence packing (Raffel et al., 2020), which reduces padding requirements. Moreover, we train models with forecasting capabilities over varying context and prediction lengths. Rather than defining a fixed context and prediction length, we sample 15% - 50% lengths as forecast horizon and the remaining as context horizon, for a given time series. As most probabilistic forecasting models, we minimize the negative log-likelihood of the predicted patch with respect to the ground truth.

### C.2 EVALUATION SETUP

We primarily used the LSF (Wu et al., 2023) and Monash (Godahehwa et al., 2021) datasets to evaluate the model’s out-of-distribution generalization ability. For the LSF dataset, we only used the test set and performed evaluations in a non-overlapping rolling window fashion, with the stride equal to the prediction length. For the Monash dataset, considering its large size, we set only one window per sample for evaluation. The evaluated results in Monash dataset are exhibited in Appendix D.3. The below table details the evaluation setting per dataset:

Table 3: Out-of-distribution Evaluation Datasets.

Dataset	Domain	Frequency	# Prediction Length	# Rolling Evaluations.
ETTh1	Energy	H	192	175
ETTh2	Energy	H	192	819
ETTh1	Energy	H	192	819
ETTh2	Energy	H	192	819
Electricity	Energy	H	192	7062
Weather	Climate	H	192	1029
M4 Hourly	Finance	H	48	414
M4 Daily	Finance	D	14	4227
M4 Weekly	Finance	W	13	359
M4 Monthly	Finance	M	18	48000
M4 Quarterly	Finance	Q	8	24000

Table 3 continued from previous page				
Dataset	Domain	Frequency	# Prediction Length	# Samples
M1 Monthly	Finance	M	18	617
M3 Monthly	Finance	M	18	1428
M3 Other	Finance	Q	8	174
NN5 Daily	Finance	D	56	111
NN5 Weekly	Finance	W	8	111
Tourism Monthly	Finance	M	24	366
Tourism Quarterly	Finance	Q	8	427
CIF 2016	Finance	M	6	15
Traffic Hourly	Transport	H	168	862
Traffic Weekly	Transport	W	8	862
Australian Electricity Demand	Energy	30T	336	5
Rideshare	Transport	H	168	2304
Saugeen	Climate	D	30	1
Sunspot	Climate	D	30	1
Temperature Rain	Climate	D	30	32072
Vehicle Trips	Transport	D	30	329
Weather	Climate	D	30	3010
Car Parts	Sales	M	12	2674
FRED MD	Finance	M	12	107
Pedestrian Counts	Transport	H	12	66
Hospital	Health	M	12	767
Covid Deaths	Health	D	30	266
KDD Cup 2018	Energy	H	168	270
Bitcoin	Finance	D	30	18
Us Births	Health	D	30	1

### C.3 EVALUATION METRICS

**Mean Absolute Percentage Error (MAPE).** MAPE is a commonly used metric to evaluate the accuracy of a forecasting model by expressing the error in percentage terms, making it unit-free and easily interpretable. It measures the average magnitude of the absolute percentage error between the predicted and actual values, relative to the actual values. For a univariate time series, the error is defined as:

$$e_j^{(i)} = y_j^{(i)} - \hat{y}_j^{(i)}$$

where  $y_j^{(i)}$  and  $\hat{y}_j^{(i)}$  are the target and predicted values of the  $i$ -th time series and  $j$ -th time step, respectively. The MAPE of the  $i$ -th time series is then calculated as:

$$\text{MAPE} = \frac{100}{H} \sum_{j=t+1}^{t+H} \frac{|e_j^{(i)}|}{|y_j^{(i)}|}$$

This formula calculates the percentage error at each time step, averaging it over the forecast horizon  $H$ . MAPE is intuitive and interpretable in percentage terms. However, MAPE can be highly sensi-

tive to small actual values because it divides by  $y_j^{(i)}$ , leading to extremely large errors when actual values approach zero.

**Symmetric Mean Absolute Percentage Error (sMAPE).** sMAPE addresses the shortcoming of MAPE by using a symmetric formula that normalizes both the actual and predicted values. The sMAPE of the  $i$ -th time series is defined to be

$$\text{sMAPE} = \frac{200}{H} \sum_{j=t+1}^{t+H} \frac{|e_j^{(i)}|}{|y_j^{(i)}| + |\hat{y}_j^{(i)}|}$$

The sMAPE ensures that errors are balanced between over- and under-prediction by dividing by the sum of the absolute actual and predicted values. This normalization helps avoid extreme errors when actual values are small, but it can also produce undefined results when both actual and predicted values are zero.

**Continuous Ranked Probability Score (CRPS).** Before we can introduce the CRPS, we need to introduce the weighted quantile loss Park et al. (2022), which is a metric normalized over the test set. We first define the  $\alpha$ -quantile loss, also known as the pinball loss at quantile level  $\alpha$ , to be:

$$\Lambda_\alpha(q, y) = (\alpha - 1_{y < q})(y - q)$$

The weighted quantile loss is then the normalized sum of quantile losses,

$$\text{wQL}[\alpha] = 2 \frac{\sum_{(i,j) \in \Omega} \Lambda_\alpha(\hat{q}_j^{(i)}(\alpha), y_j^{(i)})}{\sum_{(i,j) \in \Omega} |y_j^{(i)}|}$$

where  $\Omega = \{(i, j) \in \mathbb{Z}^2 : 1 \leq i \leq n, \tau_i + 1 \leq j \leq T_i\}$ .

The CRPS is a proper scoring rule Matheson & Winkler (1976), meaning that it is minimized when the predictive distribution is equal to the distribution from which the data is drawn.

$$\text{CRPS} = \int_0^1 2\Lambda_\alpha(F^{-1}(\alpha), y) d\alpha$$

However, we are unable to evaluate this quantity since we generally are not able to compute the integral in closed form and only have access to a finite number of quantile predictions. The approximation of the CRPS is an average of the weighted quantile loss over  $K$  quantiles, and thus is also known as the mean weighted quantile loss.

$$\text{CRPS} \approx \frac{1}{K} \sum_{k=1}^K \text{wQL}[\alpha_k]$$

## D ADDITIONAL RESULTS

### D.1 EMERGENT BEHAVIORS

Fig. 8 presents case studies on "emergent abilities" of TSFMs for out-of-distribution (OOD) predictions. As model size increases, one would expect the MAPE to follow a smooth power-law decline, indicating continuous improvement. However, the plots reveal distinct phenomena, where performance changes abruptly rather than gradually. This behavior is akin to the "emergent behaviors" described in (Wei et al., 2022), where certain capabilities absent in smaller models only appear in larger ones. The emergence of improved performance at certain model sizes could indicate the development of higher-order patterns or representations within the model. These emergent abilities might stem from the model's capacity to recognize and generalize complex temporal patterns that were previously inaccessible at smaller scales. Such abilities is evident particularly in zero-shot OOD predictions, where the model must extrapolate from training data to entirely unseen scenarios.

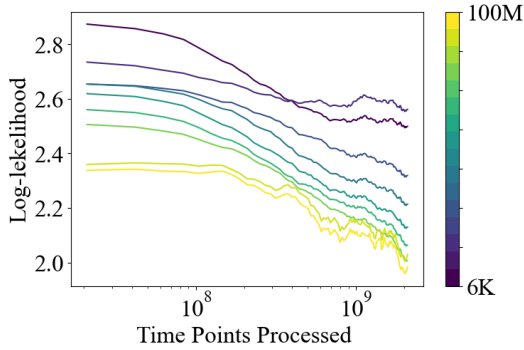


Figure 9: Training encoder-only models show that, as model scale increases, larger models require fewer samples to achieve the same level of performance.

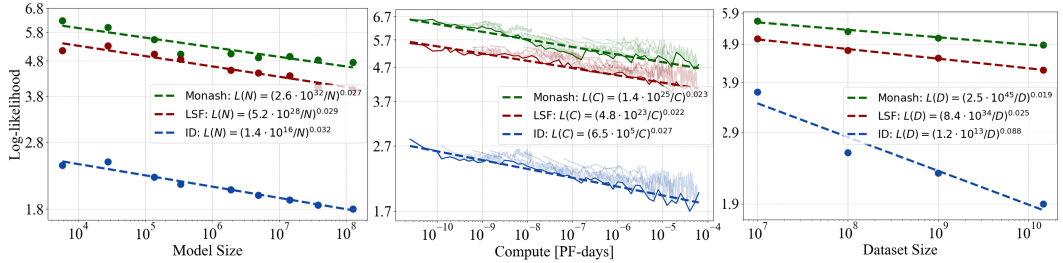


Figure 10: **Scaling Pattern Depends on Data Distributions.** The blue, red, and green plots illustrate the scaling behavior of log-likelihood loss on in-distribution (ID) data, out-of-distribution (OOD) LSF data, and OOD Monash data, respectively. We observe that the model exhibits different scaling patterns on the two different OOD datasets, indicating that OOD scaling behaviors significantly depend on the relationship between the unseen data distribution and the training data distribution.

D.2 SAMPLE EFFICIENCY

Fig. 9 illustrates the evaluation results of different-sized encoder-only models on a validation set during training. The key observation is that larger models achieve better performance with fewer training steps compared to smaller models, demonstrating higher sample efficiency. This is important in scenarios where data are limited, as larger models can achieve superior performance without processing as much data.

D.3 SCALING PATTERN DEPENDS ON DATA DISTRIBUTIONS

Fig. 10 highlights the influence of different data distributions on the scaling behavior of the model. By comparing the green line, representing the Monash dataset, and the red line, representing the LSF dataset, we observe a relatively consistent offset and similar slopes across the scaling curves. This suggests that, when transferring the model from the training data distribution to other OOD distributions, there is a predictable decrease in performance that varies by the dataset. However, the model’s gains from scaling—whether by increasing model size, compute, or dataset size—follow a fixed proportional relationship. This indicates that while OOD performance degrades, scaling the model still yields a consistent improvement ratio across different distributions, albeit with varying levels of absolute performance. Moreover, in the future, we can further analyze the reasons why transfer cost arises and establish a law to predict the transfer performance loss in population-risk based theoretical analysis (Yang et al., 2021) through Wasserstein measurement.



#### D.4 SCALING PATTERN DEPENDS ON PERFORMANCE METRICS

We investigate the scaling behaviors of five common performance metrics: log-likelihood, MAPE, CRPS, sMAPE and MAE(as shown in Figures 11 12 and 13). All metrics exhibit a decreasing trend following an approximate power-law; however, each metric demonstrates distinct scaling characteristics, reflected in their varying power-law exponents. Previous work by Ghorbani et al. (2021) establishes a relationship between large language models’ log-likelihood loss and the BLEU score in translation tasks. Similarly, future research could explore a transformation between log-likelihood loss and time series forecasting metrics, offering a means to predict forecasting performance from training loss.

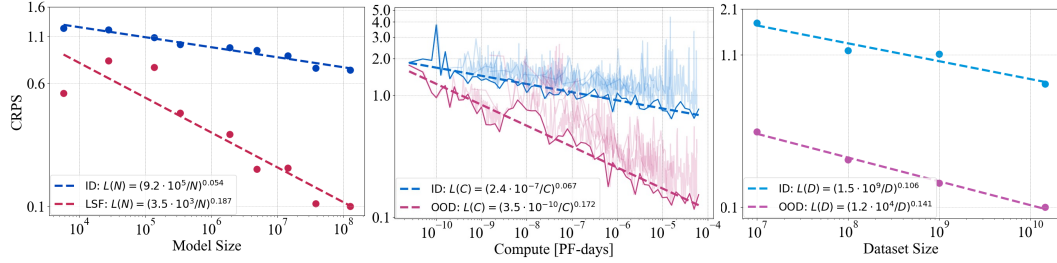


Figure 11: **Scaling Pattern of CRPS.** This figure illustrates scaling laws for CRPS across three training factors: model size, compute, and dataset size. The blue plots indicate the ID performance, while the red plots represent OOD performance. In both ID and OOD scenarios, CRPS decreases with the three factors scaling up.

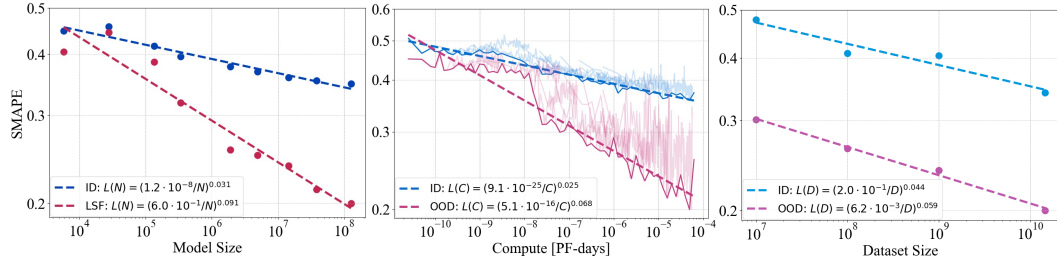


Figure 12: **Scaling Pattern of sMAPE.** This figure presents the scaling laws for sMAPE in relation to three training factors: model size, compute, and dataset size. The blue plots show performance in ID scenarios, while the red plots depict OOD performance. In both cases, sMAPE decreases as all three factors increase.

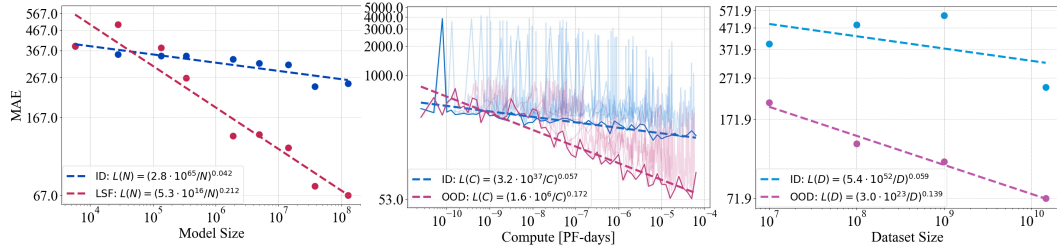


Figure 13: **Scaling Pattern of MAE.** This figure illustrates scaling laws for MAE in relation to model size, compute, and dataset size. The blue lines represent ID performance, while the red lines show OOD performance. In all cases, increasing model size, compute, or dataset size reduces MAE, with out-of-distribution performance improving more significantly.